



# Investigation of sources of gravity waves observed in the Brazilian Equatorial region on 08 April 2005

Oluwakemi Dare-Idowu<sup>1,2</sup>, Igo Paulino<sup>1</sup>, Cosme A. O. B. Figueiredo<sup>3</sup>, Amauri F. Medeiros<sup>1</sup>, Ricardo A. Buriti<sup>1</sup>, Ana Roberta Paulino<sup>1,4</sup>, and Cristiano M. Wrasse<sup>3</sup>

5 <sup>1</sup>Unidade Acadêmica de Física, Universidade Federal de Campina Grande, Campina Grande, 58429-900, Brazil

<sup>2</sup>University of Paul Sabatier, Toulouse, 31330, France

<sup>3</sup>Divisão de Aeronomia, Instituto Nacional de Pesquisas Espaciais, São José dos Campos, 12227-010, Brazil

<sup>4</sup>Departamento de Física, Universidade Estadual da Paraíba, Campina Grande, 58429-500, Brazil

10 **Correspondence:** Oluwakemi Dare-Idowu (oluwakemidareidowu@gmail.com)

## Abstract.

On 08 April 2005, a strong gravity wave activity (more than 3 hours) was observed in São João do Cariri (7.4° S, 36.5° W). These waves propagated to the southeast and presented different spectral characteristics (wavelength, period and phase speed). Using OH airglow images, the parameters of 5 observed gravity waves were calculated; the wavelengths ranged from  
15 90 to 150 km, the periods from ~26 to 67 min and the phase speeds ranged between 32 to 71 m/s. A [reverse](#) ray-tracing analysis was performed to research the possible sources of these detected waves. The ray-tracing database was composed of temperature profiles from NRLMSISE-00 model and SABER measurements and wind profiles from HWM model and meteor radar data. According to the ray path, the likely source of these observed gravity waves was the Inter Tropical Convergence Zone with intense convective processes taking place in the northern part of the observatory. Also, the observed preferential  
20 propagation direction of the waves to the southeast could be explained using blocking diagrams, i.e. due to the wind filtering process.

**Keywords.** Gravity waves, Airglow, Reverse Ray Tracing, Troposphere, Mesosphere, ITCZ.

## 1. Introduction

Since the publication of the pioneering works of Hines in the 1960s on the [climatic influence of gravity waves \(GWs\)](#),  
25 there have been numerous improvement work-outpours. Gravity waves are results of disturbances that occur in atmospheric fluids with the upper mesosphere and thermosphere region being largely impacted (e.g., Fritts and Alexander, 2003). Potential sources of these waves are cold fronts (e.g Plougonven et al., 2017), troposphere convection (e.g., Vadas et al., 2009), wind shear (e.g Clemesha and Batista, 2008), topography and wave breaking (e.g., Sarkar and Scotti, 2017) [and](#) solar eclipse (e.g Marlton et al., 2016) [as well](#).



Internal GWs are generated as adjustment radiations whenever a sudden change in forcing causes the atmosphere to depart from its large-scale balanced state. Such a forcing anomaly occurs during a solar eclipse (Marlton et al., 2016).

To identify source location of gravity waves, the reverse ray tracing method has been widely adopted. This algorithm allows the identification of the source locations of gravity waves. Several researchers have successfully implemented this technique to identify points of generation of these gravity waves under the influence of atmospheric conditions using airglow images from all sky imagers (e.g., Hecht et al., 1994; 1997; Brown et al., 2004; Wrasse et al., 2006; Vadas et al., 2009; Pramitha et al., 2014, Sivakandan et al., 2016).

Wrasse et al., (2006) did a comprehensive study of gravity waves observed over Brazil and Indonesia and concluded that most of the studied rays have their sources in the troposphere. Similarly, Vadas et al. (2009) studied the propagation of gravity waves observed during the SpreadFEx campaign in Brazil and found out that the likely sources for those waves was deep convection in Brazil. Pramitha et al., (2014) also identified that 64 % of observed GWs over Gadanki, India originated from the upper troposphere while the remaining was seen to have been ducted in the mesosphere. Sivakandan et al. (2016) also studied Gws observed in the southern part of India and associated the sources to the convection.

The objective of this present study is to extensively study a strong activity of GWs observed in São João do Cariri (7.4° S, 36.5° W) on 08 April 2005. More than three hours of GW activities were observed and the waves propagated exclusively to the southeast. An explanation for this uncommon pattern is presented in this work investigating the combining effect of the location of the source and the wind filtering process.



## 2. Instrumentation

### 2.1 The all sky imager

The GWs detected in this study were observed using the All Sky CCD Imager (ASI) installed at the observatory in São João do Cariri. The ASI is an optical instrument that provides monochromatic maps of aurora and atmospheric airglow emission of different wavelengths. It has been designed to keep track of the spatial and temporal variations of OH, OI5577, 6300 nm airglow emissions (e.g. Paulino et al., 2010).

This present study however utilized only the OH airglow images captured by the ASI at altitude of 87 km. This instrument comprises of a fish-eye (f/4) lens that captures all-sky images, it has a telecentric lens system, a computer-controlled filter wheel with several slots for the different emissions, and a charged coupled device (CCD) camera with a CCD device used as a photodetector for increased sensitivity. More technical and operational details about this particular imager at São João do Cariri can be found in Paulino et al. (2012).

### 2.2 TIMED/SABER Satellite

The Sounding of the Atmosphere using Broadband Emission Radiometry (SABER) is one of the four instruments onboard the Thermosphere Mesosphere Ionosphere Energetics and Dynamics (TIMED) satellite. This instrument measures the



vertical temperature profile of the atmosphere. In this study, temperature measurements from 20 to 108 km were obtained from SABER. Data from the Naval Research Laboratory Mass-Spectrometer-Incoherent-Scatter (NRLMSISE00) atmospheric model (Picone et al., 2002) was utilized for complementing the measurements at unavailable heights of 0-19 km, and 109-400 km. This instrument measures the temperature in the mesosphere-lower thermosphere (MLT) region. These measurements were used to provide vertical profiles of kinetic temperature, pressure, geopotential height, and volume mixing ratios for the trace species (Mertens et al., 2001).

### 2.3 The SKiYMET Meteor Radar

This system provided measurements of the horizontal wind speeds and direction of the mesosphere (81-99 km). The radar which is composed of Yagi antennas- 5 receiving antennas and one transmitting antenna operates at 35.24 MHz with a maximum power of 12 kW. This instrument measures radial velocity by transmitting radiations scattered from meteor trails. The phase delay between the transmitted and received signal is used to determine the position of the trail. Further detail about the radar has been published in (e.g., Hocking et al., 2001; Egito et al., 2018; Paulino et al., 2015).

## 3. Methodology and data analysis

### 3.1 Determination of gravity waves parameters

Five GW events were detected and studied as strong wave activities were observed for over three hours with preferential propagation to the southeast. To obtain their characteristics, a two-dimensional Fast Fourier Transform (FFT) was used in specified batches of OH airglow images. The pre-processing of the airglow images can be summarized in the following procedures:

- Rotating the image to fit the top of the image with the north geographic region;
- Removing low frequency waves by applying Butterworth high pass filter;
- Contrast enhancement and unwarping the airglow images.

Figure 1(a) shows one of the raw OH image obtained from the ASI in OLAP which is contaminated with stars (bright circles), and the Milky Way (white streak running from the bottom North-West to North-East direction), and tall tree branches/leaves (West-edge of the image) shown by the red arrow. Figure 1(b) however portrays a clearer image after image processing. Figure 1(c) represents the unwarped version of previous image. The last figure shows the spectrum of the encapsulated event. The bright red circle which depicts the amplitude of the gravity wave and its positioning also provides the propagating direction of the wave. Table 1 presents the observed wave events on the night of observation.

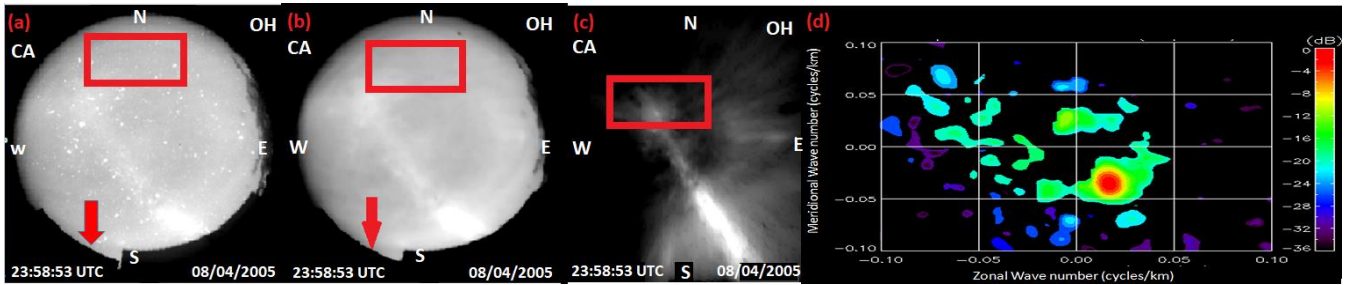


**Figure 1:** Illustration of the image processing. (a) Raw OH image collected from the ASI in São João do Cariri on 08 April 2005 (b) Filtered image (c) Unwarped image of the gravity wave event inside the red box area in previous images (d) Cross spectrum applied to the GW enclosed in the box in (c).

**Table 1:** The observed properties of the 5 wave events

Event	Time (UTC)	$\tau$ (min)	$\lambda_H$ (km)	Propagation direction ( $^\circ$ )	$cH$ (ms $^{-1}$ )
01	20:22	26.3	90.2	139.8	57.2
02	21:33	66.9	144.5	131.2	36.0
03	22:56	64.2	125.8	125.0	32.7
04	23:29	40.8	142.0	142.0	58.0
05	23:58	35.0	149.2	150.9	71.0

### 3.2 The atmospheric profile

The SABER instrument provided temperature measurement from 23:46-23:51 UT on 08 April, and from 8:35-08:40 UT on 09 April for altitudes 20-108 km. Linear interpolation was done to construct 13 profiles with a temporal resolution of 2hrs while using the NRLMSIS model as supplements for missing heights (0-19 km, 109-400 km). However, some discrepancies were at the combining points, and so the data was smoothed so that the model can seamlessly match the measurements at these junctions. This methodology was discussed by Paulino et al. (2012) as well. The temporal and spatial variation of the temperature (not shown) with a contour interval of 154 km shows an outbreak of cold air at heights lesser than 150 km (< 300K). The peak period between 17:00 h and 19:00 h has a temperature value 1000 K.

The SKYiMET radar provided the zonal and meridional wind measurements from 81-99 km every 3 km. Similarly, numerical interpolation provided the spatial resolution of the wind with a 2 hours resolution as the temperature with supporting data from the Horizontal Wind Model (HWM) (Drob et al., 2008) from 0 km to 80 km, and above 100 km.

From the temperature and wind measurements, other atmospheric parameters representing the atmospheric state of the period of study were obtained. The pressure  $P(z) = P_0 \exp\left(-\int_0^z \frac{g}{RT} dz'\right)$  was obtained using a combination of the ideal



gas law  $P = R\rho T$  and the hydrostatic balance equation  $\frac{dP}{dz} = -g\rho$ . Where  $\rho$  is the density,  $T$  is the temperature,  $g$  is the acceleration due to gravity,  $R=8.314/X_{MW}$  is the gas constant,  $z$  is the altitude,  $P_0$  is the static pressure, and  $X_{MW}$  is the average molecular weight of the atmospheric species.

The scale height  $H = -\rho/d\rho/dz$  is obtained from the ratio of the density to the derivative with respect to the altitude, while the potential temperature is  $\theta = T(P_0/P)^{R/c_p}$ . Brunt-Väisälä frequency is  $N = \sqrt{\left(\frac{g}{\theta} \frac{d\theta}{dz}\right)}$ . See further details in Vadas et al., (2009).

### 3.3 The Reverse Ray Tracing technique

Every gravity waves gets influenced by the atmospheric winds with velocity  $\mathbf{V} = (U, V, W)$  according to the following equations:

$$10 \quad \frac{dx_i}{dt} = -k_j \frac{\partial V_j}{\partial x_i} - \frac{\partial \omega_{Ir}}{\partial x_i} \quad (1)$$

and

$$\frac{dk_i}{dt} = -V_i + \frac{(\partial \omega_{Ir})}{k_i} = -V_i + c_{gi} \quad (2)$$

where  $x_i$  is the spatial position of the wave according to the spatial component ' $i$ ',  $\omega_{Ir}$  is the real part of the intrinsic frequency and  $c_g$  is the group velocity. Equation 1 describes the ray path while the refraction of the wave vector along the ray is explained by Equation 2. The derivatives of the group velocities and the complete dispersion relation can be found in Vadas and Fritts (2005) and Vadas (2007).

Four differential equations were obtained above. These equations alongside with Equation 1 and Equation 2 were solved numerically using Runge Kutta fourth order. All the observed and intrinsic properties of the gravity waves and parameters representing the atmospheric condition were fed into the reverse ray-tracing (RRT) model. The four stopping conditions imposed constantly checks out the horizontal phase speed with the background winds. When any of the condition is violated, the ray tracing integration is terminated. The stopping criteria are: (i) sound speed greater than 90 % of the local sound speed; (ii) real part of the intrinsic frequency greater or equal to zero; (iii) vertical wavelength greater than viscosity length or dissipation of the gravity waves.

## 4. Results and discussions

### 25 4.1 Spectral Analysis Result

The spectral result shows an observed wavelength with a standard deviation of 24 km and mean value of 130 km with a large amount of variability among the observed waves. This result agrees with the results of Medeiros et al., (2007) for



waves detected in the São João do Cariri observatory. Thus, it can be confidently concluded that the observed wavelengths are good proxies for the gravity waves in this observatory.

Figure 2 shows the traveling direction of the 5 events. From the polar chart, it is seen that all the waves are propagating Southeast with an approximate azimuth of  $\sim 134^\circ$  from the north. ~~It was observed that the GWs have a preferential southeast propagation directions.~~ This is in favorable agreement with the results obtained from previous studies for the same observatory (Essien et al. 2018). This anisotropy will be discussed later on in this study.

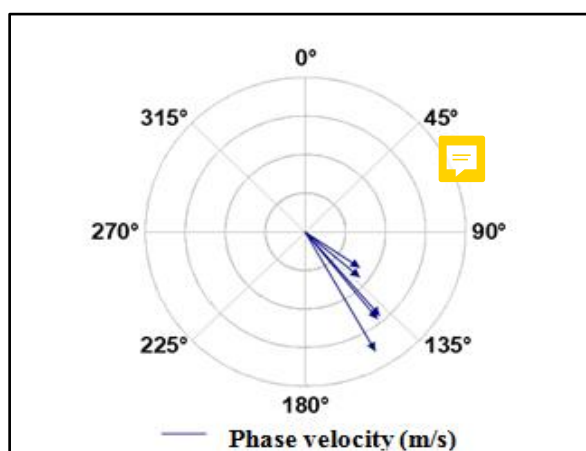


**Figure 2:** Compass graph showing wave velocities and direction of propagation.

Figure 3 shows the impact of the atmospheric wind on the period of the waves. It reveals the difference between the intrinsic period of the waves which lacks atmospheric impact and the observed period with atmospheric-winds influence. However, it can be seen that the wind accelerated all the gravity waves. The fluctuation in the period can be attributed to the variability of the horizontal winds. When the gravity wave is traveling anti-parallel to the wind direction, the second term on the left side of equation  $\omega_l = \omega_o - k_H \cdot V_{GW}$  would become negative, perpetually forcing the observed frequency to be smaller than the intrinsic frequency, this invariably results in increased observed periods.

#### 4.2 Reverse ray-tracing

These 5 waves have different spectral characteristics and they were all observed at different times as well. Ray tracing these distinct GWs back in time from the location of observation in the OH airglow layer to the possible point of generation in the lower troposphere, we show the following results. During the backward tracing, we assumed critical levels are not encountered as explained in section 3.3.

The a-panels of Fig. (4-8) are the ray-paths as a function of the altitude and time and it describes the influence of various wind conditions on each GW event. The light blue line indicates the trajectory of the gravity wave under zero wind influence, while the black line shows the travel path of the wave under the HWM wind influence. This gave a better



understanding of the roles played by the atmospheric winds in the traveling paths of GWs from the middle to the lowest atmosphere. The shaded circles points to the generation height and generation time of these waves under different wind scenarios showing the travel trajectory, alongside with the observation period.

The b-panels of Figure 4-8, however, describe the wave path as a function of longitude-latitude; thus providing a closer view of the exact generation point of these waves linearized over the map. The dark blue clouds represent the corresponding convective processes observed at the exact time that these gravity waves were detected. The black shaded triangle represents the exact location of the ASI at the OLAP.

Figure 4(a) shows a gravity wave propagating southeastward. Under the modeled wind conditions, this wave was generated at 17:00 UT of the same day, while under zero wind influence was initiated at 16:30 UT. Thus, the atmospheric winds were favorable as it accelerated the travel speeds. The b-panel of Figure 4 zooms in on the actual source point of this wave. With a horizontal wavelength of 90 km, and phase velocity of 57.2 m/s, the reverse ray tracing results points to the source being in the northern region of the detection point (laboratory). Even though, the modeled winds and zero winds do not equal, the path taken by this wind is still on par. Below 70 km, the GW propagates rapidly in the southeast direction which could be due to the strong winds.

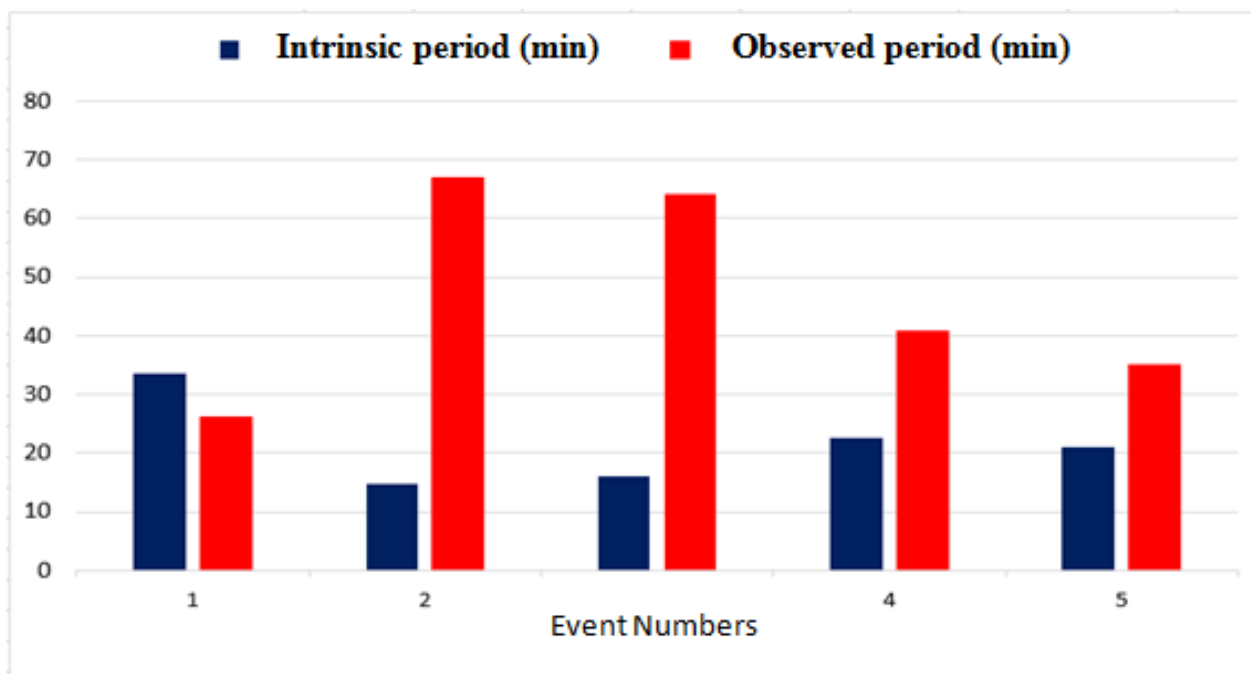
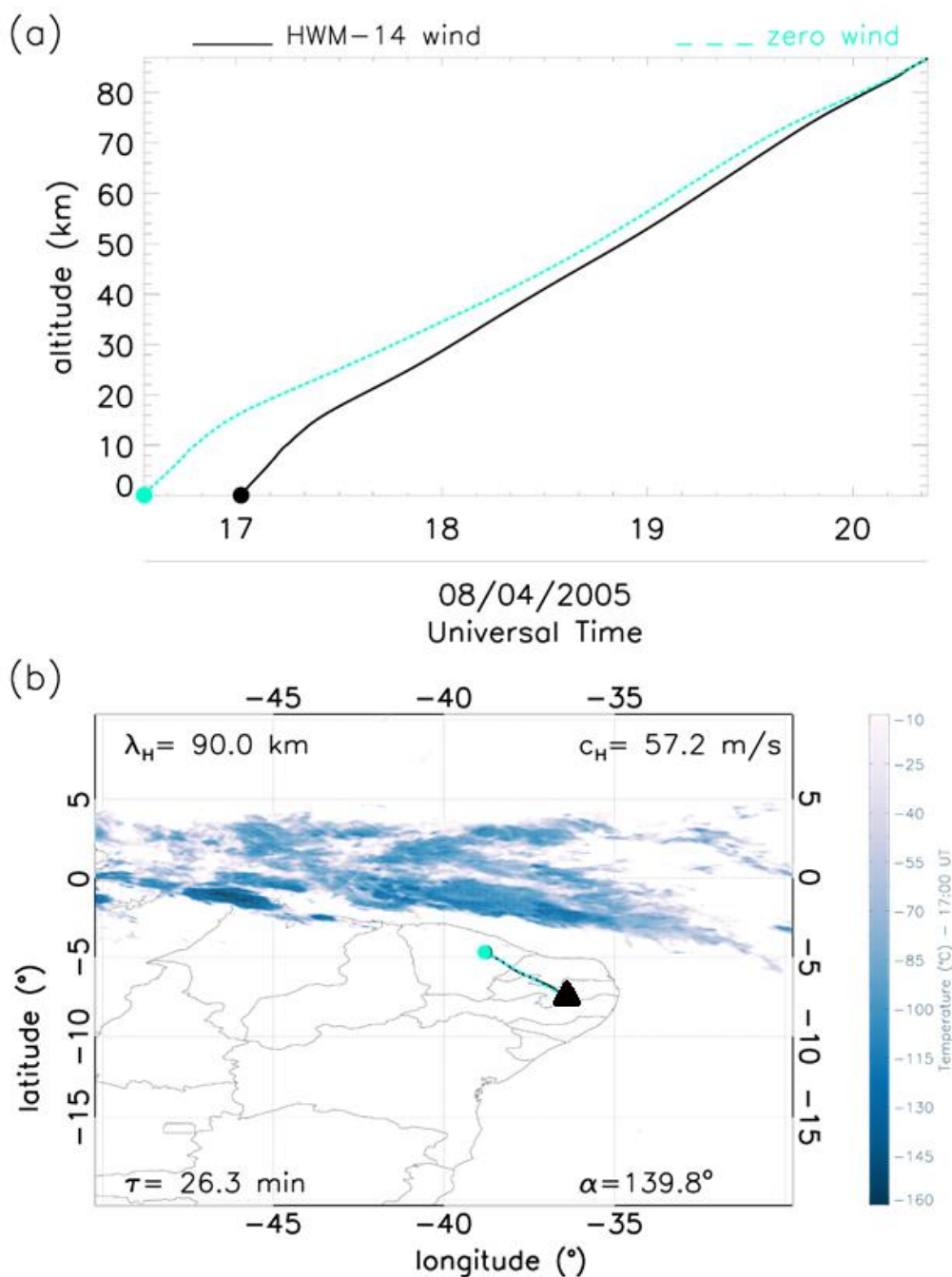


Figure 3: Bar chart graphs of intrinsic and observed periods.



**Figure 4:** Reverse ray trace results for GW 1 (a-panels: Altitude as a function of time. Dashed blue and solid black lines show the ray paths for the zero winds and modeled winds respectively, and the time cross section with zero wind and modeled winds. (b-panels: Latitude-longitude cross section over convective cloud activities). Black and blue dots show the location of sources for zero winds and modeled winds respectively. The black triangle represents the exact location of the ASI, while the blue plumes represent convective actives in the region.



Similarly, the ray-tracing results show backward propagation of the second wave event detected at 21:33 UT in Figure 5(a). This shows a similar analysis when compared to the first wave event. However, this wave suffered greater wind acceleration  $\sim 12$  hours as did  $GW_3 \sim 10$  hours. However, just as in  $GW_1$ ,  $GW_4$  and  $GW_5$  were accelerated by the modeled winds just by  $\sim 2$  hours and 1 hour respectively.

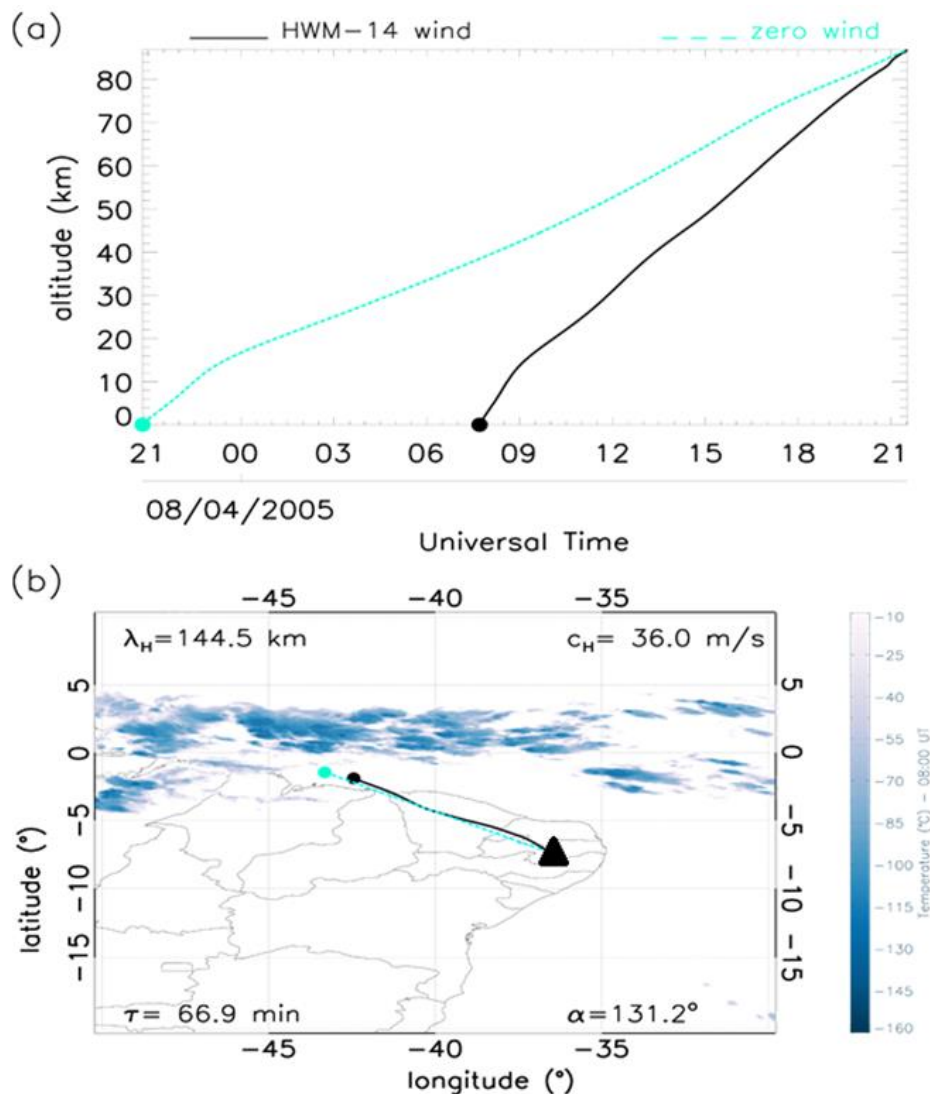


**Figure 5:** Same as Figure 4 but for Event #2.

- 5 It was observed that the events 2, 3, 4, and 5 with horizontal wavelengths of  $H \sim 140$  km propagated more than  $\sim 1300$  km from their source region. All these 4 events are believed to have originated from the same source due to the resemblance in their characteristics. Events 1, although appear to have a different but a source closer to the observatory site as it traveled a shorter



distance of ~ 700 km before detection is still source-linked to the convective processes in the ITCZ because the actual convective area is larger than the cloudy areas (Vadas and Fritts, 2009).

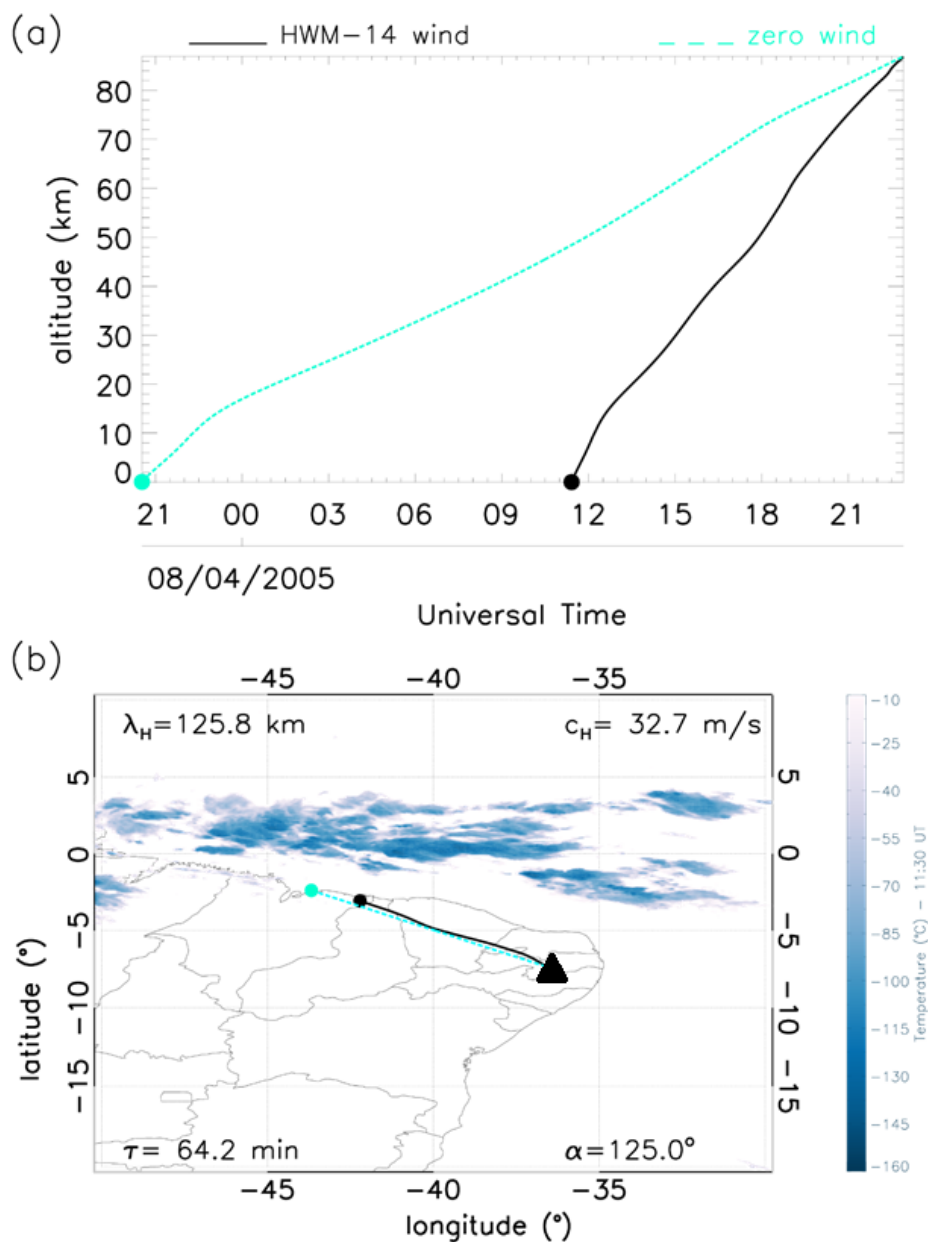


Figure 6: Same as Figure 4, but for the Event #3

5 Figures 4(b)-8(b) showed the ray paths for the wave events considering the normal and zero wind conditions. In the first panel of event 3, zero wind condition was applied, (blue line) and the modeled wind condition (black line) with a



horizontal wavelength of 90 km, phase velocity of 57.2 m/s, propagating angle of  $139.8^\circ$ , 26.3-min period and a vertical wavelength of 90.2 km. It can be noticed in panel (a) of Event #3 that the GW attained the 87 km height for both wind conditions. A slight shift can be observed as there is similarity between both conditions.

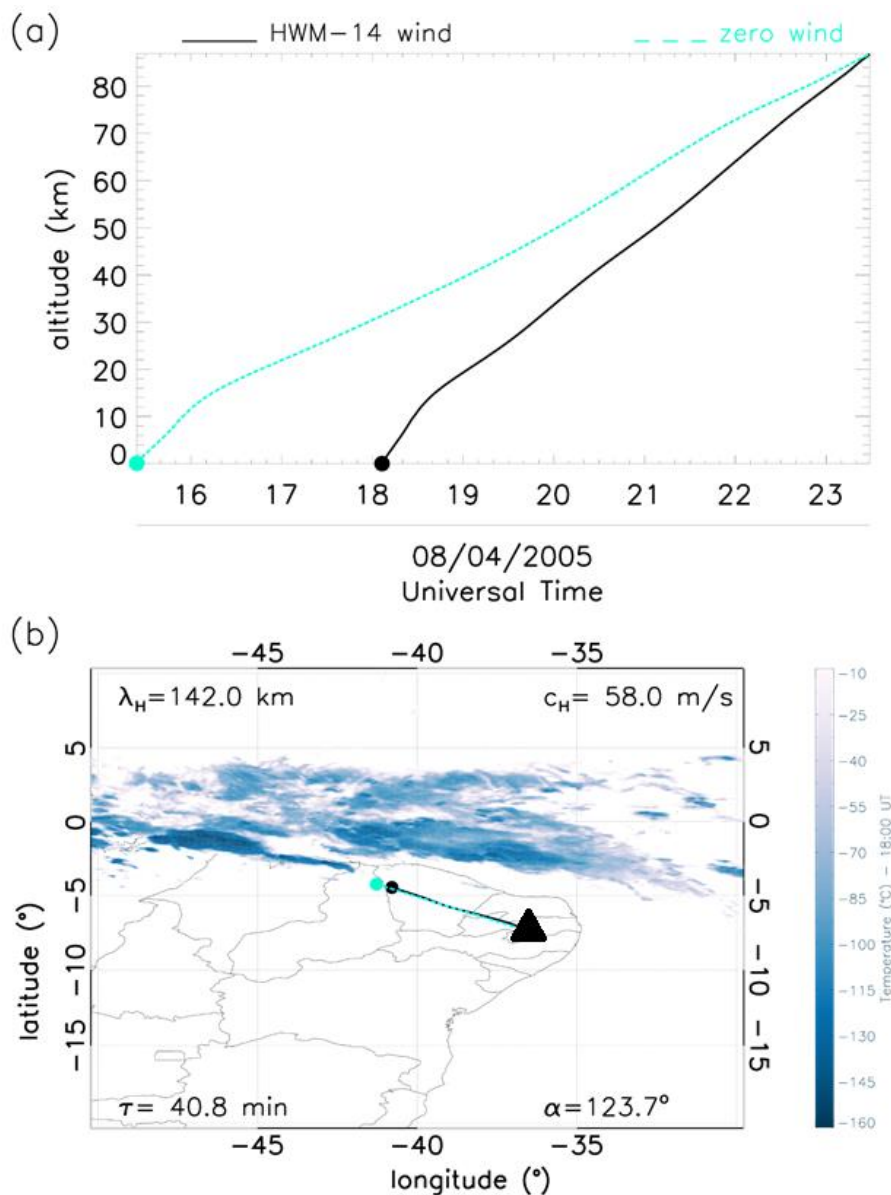
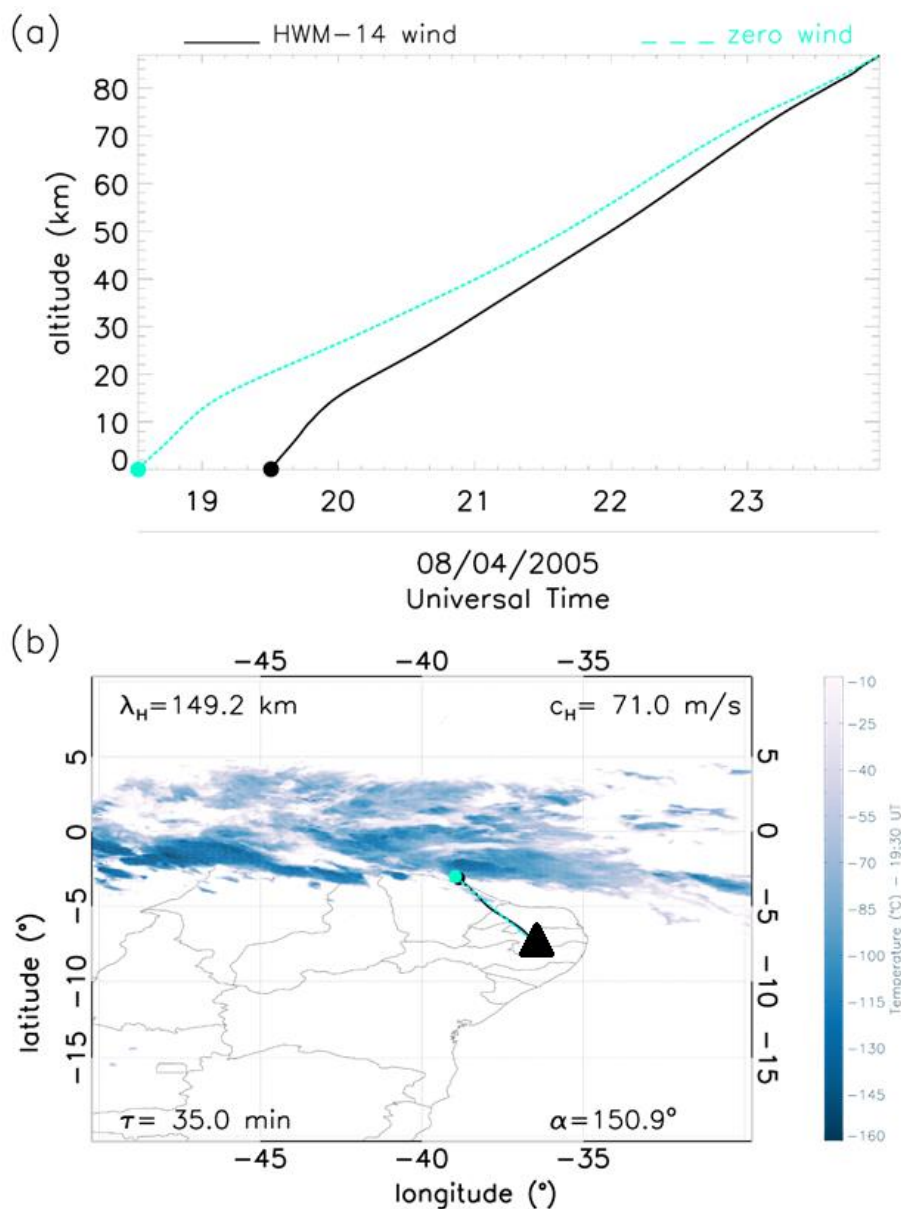


Figure 7: Same as Figure 4 but for Event #4.



**Figure 8:** Same as Figure 5 but for event #5.

The 5 wave events were reverse traced to some convection activities occurring in the northern region of the OLAP observatory. These have been identified as possible generators of these waves. One question is evident, why the propagation direction of the wave is southeastward, since the ITCZ extends horizontally to the north part of the observatory? These results are in close agreement with previous results of different studies obtained at this laboratory (e.g., Medeiros et al., 2003 and Essien et al., 2018). One should expect that the gravity waves should propagate across all and varying directions according



to the location of the ITCZ. Thus, further investigation ~~became~~ necessary to explain this anisotropy. In order to better understand the physical mechanism that is producing the anisotropy, blocking diagrams have been used to investigate the role of the wind in the filtering process of the GWs.

5 Atmospheric winds are the default features of a real atmosphere. As these gravity waves propagate in the wind direction into the upper atmosphere, they would be susceptible to the Doppler's effect and critical level dissipation (Bretherton, 1966). The critical level marks the region where the horizontal wind component annuls wave's horizontal phase speed (Medeiros et al., 2003). This region is very important as it decides how and if a traveling wave would propagate further. To understand the anisotropy of these GWs, we apply the critical level theory of the atmospheric gravity waves filtering. From Gossard and Hooke (1975) relation, the intrinsic frequency of the gravity wave under the influence of both horizontal  
10 wind components can be described by the below equation:

$$\omega_I = \mathbf{k} \cdot (\mathbf{c} - \mathbf{V}) \quad (3)$$

where  $\mathbf{k}$  is the magnitude of the horizontal wave vector,  $\mathbf{V}$  represents the two horizontal wind components, while  $c$  is the horizontal phase speeds that is observed in the detected gravity waves. Equation (3) can also be re-expressed in terms of the  
15 zonal and meridional components. Further details can be found in the works of Medeiros et al. (2003), Campos et al. (2016) and Paulino et al. (2018). **Blocking diagrams were constructed and the results are shown in the following figures.**

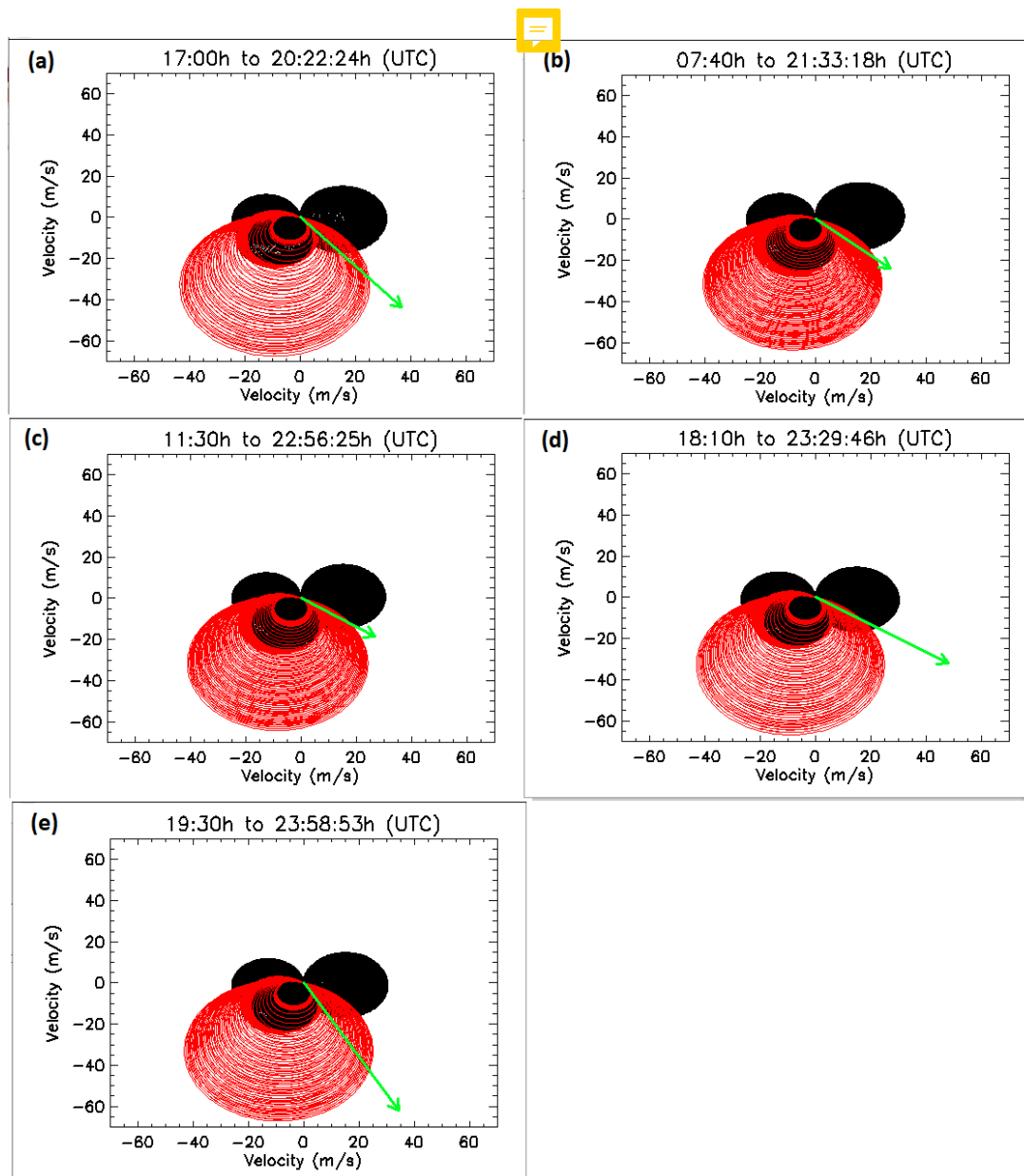


**Figure 9:** (a) Two-dimensional blocking diagrams for GW #1, (b) GW #2, (c) GW #3, (d) GW #4s, and (e) GW #5 events observed at the OH layer (87 km). The green arrow depicts the magnitude and direction of the phase velocity of each gravity wave. The shaded region represents the magnitude and the direction of the restricted area for the propagation of the wave to the (OH) layer. The meshed region in red are the measured wind measurements from the meteor radar. The black regions are the modeled wind data from the HWM model.

Constructing a polar chart as a function of the azimuthal angles and phase speeds using the wind data from HWM and the Skiyet meteor radar, we show where the phase speeds of these gravity waves equaled the wind speed of the background. The critical levels were projected into the blocking diagram showing for each horizontal wind speed and azimuths



of the corresponding GWs. If the phase speed of the GW is into the blocking lines, it represents that the wave is prohibited to propagate upwards.

The above blocking diagram allows the detection of regions where  $\omega_l \leq 0$  on the night of 08 April 2005, from 19:27 to 23:58 UT for OH emission layer and below. Every circle in this diagram shows the critical level of the vertical propagation of these waves. The red and black mesh signifies the measured and modeled wind components respectively while the green arrow represents the magnitude and direction of the detected GW. The theory of filtering process of gravity waves disallows waves propagating into the shaded region due to the effect of the critical levels (Paulino et al. 2018).

Similarly, we observed that the phase velocity of all the GW events were indeed greater in magnitude than the wind speed and so having enough momentum to skip and propagate through the critical levels easily. It is important to note the main contributions to the blocking area were due to the measured wind in the mesosphere and lower thermosphere, making this analysis strongly confident.

Thus, these detected waves avoided and escaped absorption in the forbidden regions by traveling at these interesting angles. This, with the anisotropy of the waves furthermore compels the source location of the wave to be in the Northwest. The sources of these waves were identified as the convective processes in the ITCZ zone.

## 5. Conclusions

Using the airglow images captured by the ASI at São João do Cariri, we investigated the sources of some gravity waves events detected on the night of 08 April 2005 in the OH airglow layer. Using the spectral analyzing method, we obtained the characteristics of 5 major gravity events with horizontal wavelengths concentrated between 90 km and 149 km. The phase speeds were distributed between the range of 32 m/s to 71 m/s, and the observed periods extended from 26 min to 67 min. These waves presented spectral characteristics that are very compatible with waves previously observed in the same site. In addition, southeast propagation suggested possible sources in the northwest of the observatory.

Focusing on the possible sources of these waves, we back traced the trajectory of each of these waves from the OH layer (87 km) back into the troposphere using the meteor radar wind data, the HWM model winds, and zero winds. We found out that the RRT traced the source to active convective processes in the ~~Inter-Tropical Convergence Zone~~ in the northwest of the laboratory as shown in the back tracing results presented above. However, the ITCZ was extended by a long strip in the northern part of the observatory which suggested generation of other GWs that should have been observed in the south and southwest of the observatory. Thus, the construction of blocking diagrams showed that only the spectrum of waves with propagation to the southeast were able to propagate vertically to altitudes of the OH layer. Therefore, the filtering effect of gravity waves was decisive for explaining the presence of observed waves propagating to the Southeast.

*Data availability:* All sky image data used in the course of this study can be requested from Aerolume (UFCEG) or Lume (INPE) Groups by mailing igo.paulino@df.ufcg.edu.br.



*Author contributions:* OD-I has written the manuscript. IP has revised the manuscript and supervised the research. CAOBF has calculated the deep cloudy convection over the OLAP area. ARP has provided wind measurements from the meteor radar, and revised the manuscript. RAB and AFM have revised the full text. CMW has provided the spectral analysis for the observed gravity waves.

5 *Competing interests:* All the authors declare that they do not have any competing interests.

*Acknowledgements.* O. Dare-Idowu sincerely thanks the Coodenação de Aperfeiçoamento de Pessoal de nível Superior for the scholarship during her Masters program in UFCG. I. Paulino gives special gratitude to the Conselho Nacional de Desenvolvimento Científico e Tecnológico (CNPq) for their financial support (303511/2017-6) and UFCG for giving their unswerving financial support during the presentation of this work at the 27th IUGG Scientific Assembly.



## References

- Bretherton, F. P.: The propagation of groups of internal gravity waves in a shear flow, *Journal of the Royal Meteorological Society*, 92(394), 466–480, <https://doi.org/10.1002/qj.49709239403>, 1966.
- 5 Brown, L. B., Gerrard, A. J., Meriwether, J. W., and Makela, J. J.: All-sky imaging observations of mesospheric fronts in OI 557.7 nm and broadband OH airglow emissions: Analysis of frontal structure, atmospheric background conditions, and potential sourcing mechanisms, *Journal of Geophysical Research D: Atmospheres*, 109(19), <https://doi.org/10.1029/2003JD004223>, 2004.
- Campos J. A. V., Paulino, I., Wrasse, C. M., Medeiros, A. F., Paulino, A. R., and Buriti, R. A.: Observations of small-scale gravity waves in the equatorial upper mesosphere, *Revista Brasileira de Geofisica*, 34(4), <https://doi.org/10.22564/rbgf.v34i4.876>, 2016.
- 10 Clemesha, B. and Batista, P.: Gravity waves and wind-shear in the MLT at 23°S, *Advances in Space Research*, 41, 1472 – 1477, <https://doi.org/https://doi.org/10.1016/j.asr.2007.03.085>, 2008.
- Drob, D. P., Emmert, J. T., Crowley, G., Picone, J. M., Shepherd, G. G., Skinner, W., Hays, P., Niciejewski, R. J., Larsen, M., She, C. Y., Meriwether, J. W., Hernandez, G., Jarvis, M. J., Sipler, D. P., Tepley, C. A., O'Brien, M. S., Bowman, J. R., Wu, Q., Murayama, Y., Kawamura, S., Reid, I. M., and Vincent, R. A.: An empirical model of the Earth's horizontal wind fields: HWM07, *Journal of Geophysical Research (Space Physics)*, 113, 12 304, dOI: 10.1029/2008JA013668, 2008.
- 15 Essien P., E., Paulino, I., Wrasse, C. M., Campos, J. A. V., Paulino, A. R., Medeiros, A. F., and Buriti, R. A.: Seasonal characteristics of small- and medium-scale gravity waves in the mesosphere and lower thermosphere region over Brazilian equatorial sector, *Annales Geophysicae*, (Submetid), 1–26, <https://doi.org/10.5194/angeo-36-899-2018>, 2018.
- 20 Fritts, D. C. and Alexander, M. J.: Gravity wave dynamics and effects in the middle atmosphere, *Reviews of Geophysics*, 41, n/a–n/a, <https://doi.org/10.1029/2001RG000106>, 1003, 2003.
- Gossard, E. and Hooke, W.: *Waves in the atmosphere: atmospheric infrasound and gravity waves- their generation and propagation*, Elsevier Scientific Publishing Co., 1975.
- 25 Hecht, J. H., Walterscheid, R. L., and Ross, M. N.: First measurements of the two-dimensional horizontal wave number spectrum from CCD images of the nightglow, *Journal of Geophysical Research*, 99(A6), 11449, <https://doi.org/10.1029/94JA00584>, 1994.



- Hocking, W. K., Fuller, B., and Vandeppeer, B.: Real-time determination of meteor-related parameters utilizing modern digital technology, *Journal of Atmospheric and Solar-Terrestrial Physics*, 63(2–3), 155–169, [https://doi.org/10.1016/S1364-6826\(00\)00138-3](https://doi.org/10.1016/S1364-6826(00)00138-3), 2001.
- Marlton, G. J., Williams, P. D., and Nicoll, K. A.: On the detection and attribution of gravity waves generated by the 20  
5 March 2015 solar eclipse, <https://doi.org/10.1098/rsta.2015.0222>, 2016.
- Medeiros, A. F., Taylor M. J., Takahashi, H., Batista, P. P., and Gobbi, D.: An investigation of gravity wave activity in the low-latitude upper mesosphere: Propagation direction and wind filtering, *Journal of Geophysical Research: Atmospheres*, 108, <https://doi.org/10.1029/2002JD002593>, 2003.
- Medeiros, A. F., Takahashi, H., Buriti, R. A., Fechine, J., Wrasse, C. M., and Gobbi, D.: MLT gravity wave climatology  
10 in the South America equatorial region observed by airglow imager, *Annales Geophysicae*, 25, 399–406, <https://doi.org/10.5194/angeo-25-399-2007>, 2007.
- Mertens, C. J., Mlynczak, M. G., López-Puertas, M., Wintersteiner, P. P., Picard, R. H., Winick, J. R., Gordley, L. L., and Russell III, J. M.: Retrieval of mesospheric and lower thermospheric kinetic temperature from measurements of CO<sub>2</sub> 15  
15  $\mu\text{m}$  Earth Limb Emission under non-LTE conditions, *Geophysical Research Letters*, 28, 1391–1394, <https://doi.org/10.1029/2000GL012189>, 2001.
- Nyassor P. K., Buriti, R. A., Paulino, I., Medeiros, A. F., Takahashi, H., Wrasse, C. M., and Gobbi, D.: Determination of gravity wave parameters in the airglow combining photometer and imager data. *Annales Geophysicae*, 36(3), 705–715, <https://doi.org/10.5194/angeo-36-705-2018>, 2018.
- Paulino, A., Batista, P., Lima, L., Clemesha, B., Buriti, R., and Schuch, N.: The lunar tides in the mesosphere and lower  
20 thermosphere over Brazilian sector, *Journal of Atmospheric and Solar-Terrestrial Physics*, 133, 129 – 138, <https://doi.org/https://doi.org/10.1016/j.jastp.2015.08.011>, 2015.
- Paulino, A. R., Batista, P. P., and Batista, I. S.: A global view of the atmospheric lunar semidiurnal tide, *Journal of Geophysical Research: Atmospheres*, 118, 13,128–13,139, <https://doi.org/10.1002/2013JD019818>, 2013.
- Paulino, I., Medeiros, A., Buriti, R., Sobral, J., Takahashi, H., and Gobbi, D.: Optical observations of plasma bubble  
25 westward drifts over Brazilian tropical region, *Journal of Atmospheric and Solar-Terrestrial Physics*, 72, 521 – 527, <https://doi.org/https://doi.org/10.1016/j.jastp.2010.01.015>, 2010.



- Paulino, I., Takahashi, H., Vadas, S., Wrasse, C., Sobral, J., Medeiros, A., Buriti, R., and Gobbi, D.: Forward ray-tracing for medium-scale gravity waves observed during the {COPEX} campaign, *Journal of Atmospheric and Solar-Terrestrial Physics*, 90-91, 117 – 123, <https://doi.org/10.1016/j.jastp.2012.08.006>, recent Progress in the Vertical Coupling in the Atmosphere-Ionosphere System, 2012.
- 5 Paulino, I., Moraes, J. F., Maranhão, G. L., Wrasse, C. M., Buriti, R. A., Medeiros, A. F., Paulino, A. R., Takahashi, H., Makela, J. J., Meriwether, J. W., and Campos, J. A. V.: Intrinsic parameters of periodic waves observed in the OI6300 airglow layer over the Brazilian equatorial region, *Annales Geophysicae*, 36, 265–273, <https://doi.org/10.5194/angeo-36-265-2018>, <https://www.ann-geophys.net/36/265/2018/>, 2018.
- Picone, J. M., Hedin, A. E., Drob, D. P., and Aikin, A. C.: NRLMSISE-00 empirical model of the atmosphere: Statistical comparisons and scientific issues, *J. Geophys. Res.*, 107, 1468, 0148-0227, 2002.
- 10 Plougonven, R., Jewtoukoff, V., Cámara, A. d. I., Lott, F., and Hertzog, A.: On the Relation between Gravity Waves and Wind Speed in the Lower Stratosphere over the Southern Ocean, *Journal of the Atmospheric Sciences*, 74, 1075–1093, <https://doi.org/10.1175/JAS-D-16-0096.1>, 2017.
- 15 Pramitha, M., Venkat Ratnam, M., Taori, A., Krishna Murthy, B. V., Pallamraju, D., and Vijaya Bhaskar Rao, S.: Identification of gravity wave sources using reverse ray tracing over Indian region, <https://doi.org/10.5194/acpd-14-19587-2014>, 2014.
- Sarkar, S., and Scotti, A.: Topographic Internal Gravity Waves to Turbulence, *Annual Review of Fluid Mechanics*, 49(1), 195–220. <https://doi.org/10.1146/annurev-fluid-010816-060013>, 2017.
- 20 Sivakandan, M., Paulino, I., Taori, A., and Niranjana, K.: Mesospheric gravity wave characteristics and identification of their sources around spring equinox over Indian low latitudes, 9(1), 93–102, <https://doi.org/10.5194/amt-9-93-2016>, 2016.
- Vadas, S. L. and Fritts, D. C.: Thermospheric responses to gravity waves: Influences of increasing viscosity and thermal diffusivity, *Journal of Geophysical Research: Atmospheres*, 110, <https://doi.org/10.1029/2004JD005574>, 2005.
- 25 Vadas, S. L.: Horizontal and vertical propagation and dissipation of gravity waves in the thermosphere from lower atmospheric and thermospheric sources, *Journal of Geophysical Research: Space Physics*, 112, <https://doi.org/10.1029/2006JA011845>, 2007.



Vadas, S. L. and Fritts, D. C.: Reconstruction of the gravity wave field from convective plumes via ray tracing, *Annales Geophysicae*, 27, 147–177, <https://doi.org/10.5194/angeo-27-147-2009>, 2009.

5 Vadas, S. L., Taylor, M. J., Pautet, P.-D., Stamus, P. A., Fritts, D. C., Liu, H.-L., São Sabbas, F. T., Rampinelli, V. T., Batista, P., and Takahashi, H.: Convection: the likely source of the medium-scale gravity waves observed in the OH airglow layer near Brasilia, Brazil, during the SpreadFEx campaign, *Annales Geophysicae*, 27, 231–259, <https://doi.org/10.5194/angeo-27-231-2009>, 2009.

10 Wrasse, C. M., Nakamura, T., Takahashi, H., Medeiros, A. F., Taylor, M. J., Gobbi, D., Denardini, C. M., Fechine, J., Buriti, R. A., Salatun, A., Suratno, A., Achmad, E., and Admiranto, A. G.: Mesospheric gravity waves observed near equatorial and low and middle latitude stations: wave characteristics and reverse ray tracing results, *Annales Geophysicae*, 24, 3229–3240, <https://doi.org/10.5194/angeo-24-3229-2006>, 2006.

Egito, Fabio & Arlen Buriti, Ricardo & Medeiros, A & Takahashi, Hisao. (2018). Ultrafast Kelvin waves in the MLT airglow and wind, and their interaction with the atmospheric tides. *Annales Geophysicae*. 36. 231-241. [10.5194/angeo-36-231-2018](https://doi.org/10.5194/angeo-36-231-2018).